

Two-point functions of quenched lattice QCD in Numerical Stochastic Perturbation Theory. (II) The gluon propagator in Landau gauge

F. Di Renzo

Dipartimento di Fisica, Università di Parma and INFN, I-43100 Parma, Italy

E.-M. Ilgenfritz

Fakultät für Physik, Universität Bielefeld, D-33501 Bielefeld, Germany

Institut für Physik, Humboldt-Universität zu Berlin, D-12489 Berlin, Germany

H. Perlt, A. Schiller

Institut für Theoretische Physik, Universität Leipzig, D-04009 Leipzig, Germany

C. Torrero

Institut für Theoretische Physik, Universität Regensburg, D-93040 Regensburg, Germany

October 8, 2018

Abstract

This is the second of two papers devoted to the perturbative computation of the ghost and gluon propagators in $SU(3)$ Lattice Gauge Theory. Such a computation should enable a comparison with results from lattice simulations in order to reveal the genuinely non-perturbative content of the latter. The gluon propagator is computed by means of Numerical Stochastic Perturbation Theory: results range from two up to four loops, depending on the different lattice sizes. The non-logarithmic constants for one, two and three loops are extrapolated to the lattice spacing $a \rightarrow 0$ continuum and infinite volume $V \rightarrow \infty$ limits.

1 Introduction

In [1] a three-loop computation of the ghost propagator was presented. As announced, we now report on a similar computation of the gluon propagator. The full propagators of glu-

ons and ghosts calculated on the lattice encode information about the non-perturbative vacuum properties of QCD and of pure Yang-Mills theory [2]. This requires a non-perturbative extension of the Landau gauge.

Although BRST invariance is essential for other non-perturbative approaches to non-Abelian gauge theory, there are principal difficulties to reconcile it with present-day lattice gauge fixing technology (as applied for calculating gauge-variant objects like gluon and ghost propagators) in a way avoiding the Neuberger problem (see [3] and references therein). So far, there is no generally accepted way to deal with the Gribov ambiguity in lattice simulations.

Other non-perturbative methods for calculations in the Landau gauge like Schwinger-Dyson (SD) equations [4] or the Functional Renormalization Group (FRG) [5, 6] are not explicitly taking into account (and seem not to be affected by) the complication compared to the standard Faddeev-Popov procedure that the functional integration should be restricted to the Gribov horizon. Zwanziger has argued [7] that the form of the SD equations will not be affected. Rather supplementary conditions restricting solutions should account for it. The so-called scaling solution [8, 9] has been an early result of the SD approach obtained for power-like solutions. The power behavior has been further specified in [10] and confirmed by (time-independent) stochastic quantization [11].

Concerning lattice simulations, Zwanziger proposed [12] to add nonlocal terms to the action that should control the simulation to stay within the Gribov horizon ¹. In the context of the Schwinger-Dyson approach this possibility has been analytically discussed first in Ref. [13]. Standard Monte Carlo simulations without these refinements have failed to reproduce the theoretically preferred far-infrared asymptotics of the scaling solution and have supported instead the so-called decoupling solution (see Ref. [14] and references therein). This solution has later been shown to be possible in the SD and FRG approaches with suitable boundary conditions [15], but at the expense of a conflict with global BRST invariance.

Although we can assume that NSPT remains in the vicinity of the trivial vacuum, we have to understand the present situation with respect to Monte Carlo results for gluon and ghost propagators. Fortunately, the momentum range we are interested in and where we are going to compare with Monte Carlo lattice results is not influenced by the Gribov ambiguity and the way of gauge fixing [16]. From various studies it is known, however, that the intermediate momentum range of $\mathcal{O}(1 \text{ GeV})$ is not less important from the point of view of confinement physics, as seen for the gluon propagator [17] and the quark propagator [18] in Landau gauge on the lattice. From the FRG approach it is known that for the onset of confinement at finite temperature the mid-momentum region of the propagators is important [19, 20]. This is the region where violation of positivity [17, 21, 22] invalidates a conventional, particle-like interpretation of the gluon propagator. Specific non-perturbative configurations (center vortices) have been found to be essential [17, 18] to understand the behavior of the gluon and the quark propagator in the intermediate momentum range.

In recent years, also the large-momentum behavior of the lattice gluon and ghost prop-

¹In this first attempt a singular ghost propagator $\propto 1/p^4$ has been obtained.

agators has attracted growing interest, in particular with respect to the coupling constant of the ghost-gluon vertex [23, 24, 25, 26], which has the potential to provide an independent precision measurement of $\alpha_s(M_Z)$ from these propagators [27]. First estimates of the zero- and two-flavor values of $\Lambda_{\overline{\text{MS}}}$ [24, 25, 26] and a possible dimension-two condensate [24, 26] are available already and look promising. Therefore, a detailed knowledge of the propagators' lattice perturbative part would much foster these efforts.

When our work begun in 2007 [28, 29], the intention was to clarify the perturbative background, among other facts the type of convergence of the summed-up few-loop perturbative contributions to the propagators in various momentum ranges. In standard Lattice Perturbation Theory (LPT) such calculations are very difficult beyond two-loop order. To overcome this obstacle, we have used the method of Numerical Stochastic Perturbation Theory (NSPT) [30], which provides a stochastic, automatized framework for gauge-invariant and gauge-non-invariant calculations.

Stochastic gauge fixing is built in, and a high-precision procedure has been devised to fix the gauge to Landau, at any given order. Thus, the propagators (for each lattice momentum) can be calculated in subsequent orders of perturbation theory. A limit is set only by storage limitations and machine precision. There are no truncation errors. For direct comparison with Monte Carlo results, we present the low-loop results summed up with inverse powers of the bare inverse coupling β^n . In this paper we also try, for the first time applied to the gluon propagator, to improve the convergence by applying boosted perturbation theory.

The effectiveness of NSPT relies on the fact that the parametrization of the (leading and non-leading) logarithmic terms can follow largely in accordance with standard perturbation theory. The essential difficulty left to NSPT is the computation of the constant contributions, which are in general very difficult to achieve in diagrammatic LPT.

Only the one-loop constant term was known since long [31] for the ghost and gluon propagator. Reproducing these results, which are obtained in the continuum and infinite-volume limits, was the first feasibility test for NSPT [28].

In general, at any order, NSPT results are obtained at finite lattice spacing and finite volume. A fitting procedure is needed to get the continuum ($a \rightarrow 0$) and infinite-volume ($V \rightarrow \infty$) limits. While the extraction of the first (continuum) limit relies on hypercubic-invariant Taylor series [32], a careful extraction of the second (infinite-volume) limit requires the accounting of pL contributions (p being the momentum scale relevant to the computation and L the finite extent of the lattice). In the first paper (abbreviated as I), we gave a quite comprehensive description of all this technology while applying it to the ghost propagator. In the present, second paper we are going to apply the method to an analysis of the gluon propagator.

The paper is organized as follows. Sect. 2 recalls the lattice definition of the gluon propagator, together with specific features that the calculation in the framework of NSPT contains. Sect. 3 contains the nomenclature of standard Lattice Perturbation Theory where our results have to fit in. In Sect. 4 we only briefly describe the implementation of NSPT. The interested reader will find more information of this kind in part I of this series of papers. However, we document the statistics for different lattice volumes and different orders of perturbation theory that has been collected by the Leipzig and Parma part of

the collaboration. Here we also present the raw data before and after the extrapolation to the Langevin time-step $\epsilon \rightarrow 0$ limit. In Sect. 5 we compare the results of NSPT (up to four loops) with Monte Carlo results and try to improve the convergence by boosted perturbation theory. Sect. 6 presents the fitting procedure and the final results for the leading and non-leading loop corrections. In Sect. 7 we draw our conclusions and summarize our results.

2 The lattice gluon propagator

The lattice gluon propagator $D_{\mu\nu}^{ab}(p(k))$ is the Fourier transform of the gluon two-point function, *i.e.* the expectation value

$$D_{\mu\nu}^{ab}(p(k)) = \langle \tilde{A}_\mu^a(k) \tilde{A}_\nu^b(-k) \rangle = \delta^{ab} D_{\mu\nu}(p(k)), \quad (1)$$

which is required to be color-diagonal and symmetric in the Lorentz indices μ, ν . For the definition of the lattice momenta $p_\mu(k_\mu)$, k_μ and $\hat{p}_\mu(k_\mu)$ to be used later we refer to (I-17)-(I-19).

Assuming reality of the color components of the vector potential and rotational invariance of the two-point function, the continuum gluon propagator has the following general tensor structure ²

$$D_{\mu\nu}(p) = \left(\delta_{\mu\nu} - \frac{p_\mu p_\nu}{p^2} \right) D(p^2) + \frac{p_\mu p_\nu}{p^2} \frac{F(p^2)}{p^2}, \quad (2)$$

with $D(p^2)$ and $F(p^2)$ being the transverse and longitudinal propagator, respectively. The longitudinal propagator $F(p^2)$ vanishes in the Landau gauge.

The lattice gluon propagator $D_{\mu\nu}(p(k))$ depends on the lattice four-momentum $p(k)$. Due to the lower symmetry of the hypercubic group its general tensor structure can be expected to be more complicated than (2) that holds in the continuum. Inspired by the continuum form (2) we consider as one strategy only the extraction of the following lattice scalars

$$\sum_{\mu,\nu} \hat{p}_\mu(k_\mu) D_{\mu\nu}(p(k)) \hat{p}_\nu(k_\nu), \quad \sum_{\mu} D_{\mu\mu}(p(k))$$

that should survive the continuum limit. Note, however, that additional lattice scalars could be measured as well. The first scalar vanishes exactly in lattice Landau gauge. In this gauge the second scalar function, corresponding to the transverse part of the gluon propagator in the continuum limit, is denoted by

$$D(p(k)) = \frac{1}{3} \sum_{\mu=1}^4 D_{\mu\mu}(p(k)). \quad (3)$$

On the lattice, this function is influenced by the the lower symmetry of the hypercubic group.

²Differently to the other chapters p denotes here directly the continuum Euclidean four-momentum.

In NSPT the different loop orders n (even orders in $\beta^{-1/2}$) at finite Langevin step size ε are constructed directly from the Fourier transformed perturbative gauge fields $\tilde{A}_\mu^{a,(l)}(k)$ with (see (I-6) and (I-7))

$$A_{x+\hat{\mu}/2,\mu} = \sum_{l>0} \beta^{-l/2} A_{x+\hat{\mu}/2,\mu}^{(l)}, \quad A_{x+\hat{\mu}/2,\mu}^{(l)} = \sum_a T^a A_{x+\hat{\mu}/2,\mu}^{a,(l)}. \quad (4)$$

what leads to

$$\delta^{ab} D_{\mu\nu}^{(n)}(p(k)) = \left\langle \sum_{l=1}^{2n+1} \left[\tilde{A}_\mu^{a,(l)}(k) \tilde{A}_\nu^{b,(2n+2-l)}(-k) \right] \right\rangle. \quad (5)$$

Note that already the tree-level contribution to the gluon propagator, $D_{\mu\nu}^{(0)}$, arises from quantum fluctuations of the gauge fields with $l = 1$. In addition, terms with non-integer $n = 1/2, 3/2, \dots$ in the previous equation (5) – which do not correspond to loop contributions – should vanish numerically after averaging over configurations.

Similar to the ghost propagator in paper I, we present the various orders of the gluon dressing function (or “form factor”) in two forms:

$$J^{G,(n)}(p) = p^2 D^{(n)}(p(k)), \quad \hat{J}^{G,(n)}(p) = \hat{p}^2 D^{(n)}(p(k)). \quad (6)$$

Contrary to the ghost propagator the gluon dressing function can be calculated at the same time for all possible four-momenta given by four integers – the four-momentum tuples (k_1, k_2, k_3, k_4) . This makes a calculation of the gluon propagator significantly cheaper. The tree-level result for the dressing function, $\hat{J}^{G,(0)}(p(k)) = 1$ in the limit $\varepsilon \rightarrow 0$ for all sets of tuples is non-trivial and is obtained as the result of averaging.

3 The propagator and standard Lattice Perturbation Theory

As discussed in paper I – we relate infrared singularities encountered in our finite volume NSPT calculation to powers of logarithms of the external momentum obtained in the infinite volume limit. Therefore, we need the anomalous dimension of the gluon field A_μ , the β -function and the relation between lattice bare and renormalized coupling. The procedure is outlined in detail in Section 4 of I. Here, we only repeat the essential equations and quote the final numbers. To avoid a possible mismatch of equations we add an index G for the gluon propagator case.

In the RI'-MOM scheme, the renormalized gluon dressing function $J^{G,\text{RI}'}$ is defined as

$$J^{G,\text{RI}'}(p, \mu, \alpha_{\text{RI}'}) = \frac{J^G(a, p, \alpha_{\text{RI}'})}{Z^G(a, \mu, \alpha_{\text{RI}'})}, \quad (7)$$

with the standard condition

$$J^{G,\text{RI}'}(p, \mu, \alpha_{\text{RI}'})|_{p^2=\mu^2} = 1. \quad (8)$$

The gluon dressing function $J^G(a, p, \alpha_{\text{RI}'})$ is the gluon wave function renormalization constant $Z^G(a, \mu, \alpha_{\text{RI}'})$ at $\mu^2 = p^2$.

The expansions of Z^G , J^G and $J^{G,\text{RI}'}$ in terms of the renormalized coupling $\alpha(a\mu) = (g(a\mu))^2/(16\pi^2)$ are completely analogous to (I-39)-(I-41). The gluon wave function renormalization as an expansion in the lattice coupling $\alpha_0 = N_c/(8\pi^2\beta)$ is represented as

$$Z^G(a, \mu, \alpha_0) = 1 + \sum_{i>0} \alpha_0^i \sum_{j=0}^i z_{i,j}^G (\log(a\mu))^j. \quad (9)$$

This is the expansion we can measure in NSPT.

Again we restrict ourselves to three-loop expressions for the Landau gauge in the quenched approximation. The coefficients in front of the logarithms are partly known from calculations of the gluon wave functions and the beta function in the continuum and given as follows (compare *e.g.* [33])

$$z_{1,1}^{G,\text{RI}'} = -\frac{13}{3} N_c, \quad (10)$$

$$z_{2,2}^{G,\text{RI}'} = -\frac{13}{2} N_c^2, \quad z_{2,1}^{G,\text{RI}'} = -\frac{3727}{108} N_c^2 + 3 z_{1,0}^{G,\text{RI}'} N_c, \quad (11)$$

$$z_{3,3}^{G,\text{RI}'} = -\frac{403}{18} N_c^3, \quad z_{3,2}^{G,\text{RI}'} = -\frac{5495}{36} N_c^3 + \frac{31}{2} z_{1,0}^{G,\text{RI}'} N_c^2, \quad (12)$$

$$z_{3,1}^{G,\text{RI}'} = -\frac{2127823}{3888} N_c^3 + \frac{361}{8} \zeta[3] N_c^3 - \frac{1279}{108} z_{1,0}^{G,\text{RI}'} N_c^2 + \frac{31}{3} z_{2,0}^{G,\text{RI}'} N_c.$$

The finite one-loop constant $z_{1,0}^{G,\text{RI}'}$ is known from the gluon self energy in standard infinite volume LPT [31] with the value

$$z_{1,0}^{G,\text{RI}'} = 60.3673076. \quad (13)$$

Again the constants $z_{2,0}^{G,\text{RI}'}$ and $z_{3,0}^{G,\text{RI}'}$ were not known so far. The form of the coefficients $z_{i,j}^G$ of $Z^G(a, \mu, \alpha_0)$ in (9) up to three loops can be read off directly from equations (I-51)-(I-53) replacing there all $z_{i,j}$ by $z_{i,j}^G$.

As a result, we present the gluon dressing function as function of the inverse lattice coupling β to that order

$$J^{G,3\text{-loop}}(a, p, \beta) = 1 + \sum_{i=1}^3 \frac{1}{\beta^i} J^{G,(i)}(a, p), \quad J^{G,(i)}(a, p) = \sum_{j=0}^i J_{i,j}^G (\log(ap)^2)^j, \quad (14)$$

with the one-loop coefficients

$$\begin{aligned} J_{1,1}^G &= -0.24697038, \\ J_{1,0}^G &= 0.03799544 z_{1,0}^{G,\text{RI}'} = 2.29368, \end{aligned} \quad (15)$$

the two-loop coefficients

$$\begin{aligned} J_{2,2}^G &= 0.08210781, \\ J_{2,1}^G &= -0.917978574 - 0.00938375 z_{1,0}^{G,\text{RI}'} = -1.484450, \\ J_{2,0}^G &= 0.10673710 z_{1,0}^{G,\text{RI}'} + 0.00144365 z_{2,0}^{G,\text{RI}'} = 6.443431 + 0.00144365 z_{2,0}^{G,\text{RI}'}, \end{aligned} \quad (16)$$

and the three-loop coefficients

$$\begin{aligned}
J_{3,3}^G &= -0.02963736, \\
J_{3,2}^G &= 0.62856608 + 0.00311972 z_{1,0}^{G,RI'} = 0.81689534, \\
J_{3,1}^G &= -4.06861256 - 0.06123991 z_{1,0}^{G,RI'} - 0.00035654 z_{2,0}^{G,RI'} \\
&= -7.7655009 - 0.00035654 z_{2,0}^{G,RI'} = -6.174164 - 0.246970 J_{2,0}^G, \\
J_{3,0}^G &= 0.375990 z_{1,0}^{G,RI'} + 0.00811105 z_{2,0}^{G,RI'} + 0.0000548523 z_{3,0}^{G,RI'} \\
&= 22.697532 + 0.00811105 z_{2,0}^{G,RI'} + 0.0000548523 z_{3,0}^{G,RI'}.
\end{aligned} \tag{17}$$

Let us repeat it once more: the leading logarithmic coefficients for a given order can be exclusively taken from continuum perturbative calculations. The non-leading log coefficients are influenced, however, by the finite lattice constants from corresponding lower loop orders.

4 Results of the NSPT calculations

4.1 Statistics

To obtain infinite volume perturbative loop results at vanishing lattice spacing, we have to study again the limit $\varepsilon \rightarrow 0$ and different lattice sizes N . We have used $N = 6, 8, 10, 12$ and $N = 16, 20, 32$ and studied the maximal loop order for the propagator $n_{\max} = 4$ and $n_{\max} = 2$, respectively. The accumulated statistics for the different ε 's and lattice sizes are collected in Tables 1 and 2.

ε	$N = 6$	$N = 8$	$N = 10$	$N = 12$	$N = 16$
0.01	1500	750	3000	1000	3000
0.02	1000	750	2000	1000	2000
0.03	1000	750	2000	1000	2000
0.05	1000	750	2000	1000	2000
0.07	1000	750	2000	1000	2000

Table 1: Number of gluon propagator measurements up to four loops ($N \leq 12$) and up to one loop ($N = 16$) using the Leipzig NSPT code.

The Landau gauge was defined by the condition (I-14). In the gluon propagator case we have used in the gauge fixing condition (I-20) $l_{\max} = 10$ orders of the perturbative gauge fields to obtain the propagator up to four loops in the case of the smaller volumes, and used $l_{\max} = 6$ for the bigger volumes with $N = 16, 20, 32$.

4.2 Raw data and check of vanishing contributions

In Fig. 1 we present as an example the measured dressing function $\hat{J}^{G,(n)}$ as function of $a^2 \hat{p}^2$

ε	$N = 16$	$N = 20$	$N = 32$
0.010	7436	5965	810
0.015	3053	3896	
0.020	4725	3015	715
0.040	2827	2633	835

Table 2: Number of tree-level, one- and two-loop gluon propagator measurements at lattices sizes $N = 16, 20, 32$ using the Parma NSPT code.

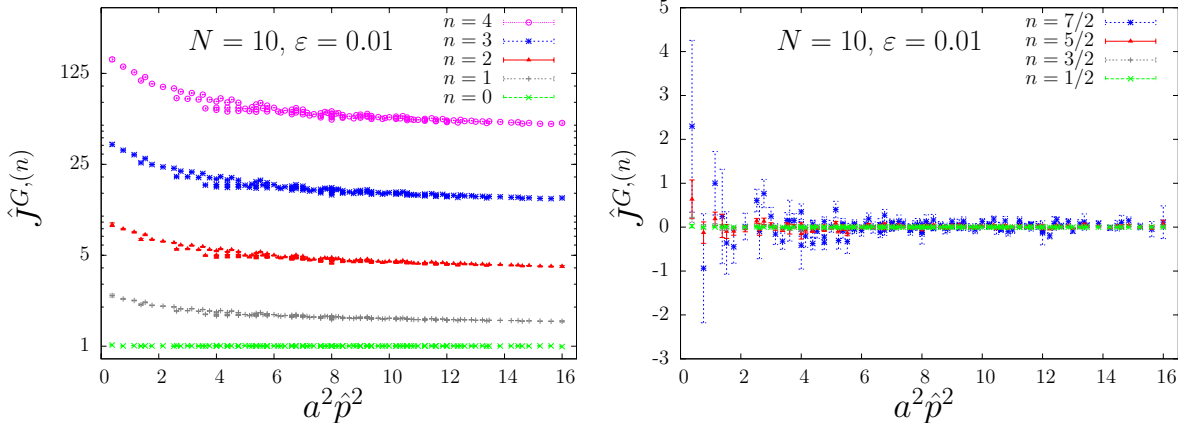


Figure 1: Raw data $\hat{J}^{G,(n)}$ vs. $a^2 \hat{p}^2$ at $N = 10$ and $\varepsilon = 0.01$. Left: Increasing loop contributions from below. Right: Vanishing non-loop contributions.

for $n = 0, 1, 2, 3, 4$ and $n = 1/2, 3/2, 5/2, 7/2$, respectively, for a lattice size 10^4 and the Langevin step $\varepsilon = 0.01$. Note that due to the hypercubic symmetry different realizations of the four-momentum tuples k can lead to the same $a^2 \hat{p}^2$ forming different branches.

In the left part of Fig. 1 the different contributions are shown starting from tree-level up to four loops. The higher loop contributions are of the same sign leading to a monotonic increase of the perturbative dressing function including higher and higher loop contributions. The right part of Fig. 1 nicely demonstrates the vanishing of the non-loop contributions. The size of the “approximate zeros” has to be compared with the corresponding sizes of the loop contributions of the “adjacent” integer loop orders.

Fig. 2 demonstrates for a chosen $n = \frac{1}{2}$ that the corresponding averages equal to zero are indeed reached at *finite* Langevin step size ε . Typically, the errors increase with decreasing step size ε and $a^2 \hat{p}^2$.

In Fig. 3 we present the result of the linear extrapolation with $\varepsilon \rightarrow 0$ for the tree-level $\hat{J}^{G,(0)}$ and one-loop $\hat{J}^{G,(1)}$ gluon dressing functions on a 16^4 lattice, together with the data of all inequivalent four-momentum tuples for $\varepsilon = 0.07$ and $\varepsilon = 0.03$, as a function of $a^2 \hat{p}^2$. Note to what precision the expected result “One” for $\hat{J}^{G,(0)}$ is reproduced.

Figs. 4 and 5 show how the one-loop and two-loop dressing functions $\hat{J}^{G,(n)}$ and $J^{G,(n)}$ depend on $a^2 \hat{p}^2$ and $(ap)^2$, respectively. The different branches for the inequivalent off-diagonal four-momentum tuples in use are clearly seen, which are strongly volume dependent.

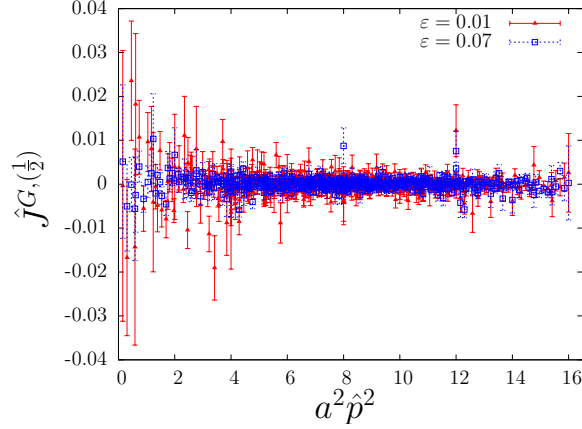


Figure 2: $\hat{j}^{G,(1/2)}$ vs. $a^2 \hat{p}^2$ at $N = 16$ and $\varepsilon = 0.01$ and 0.07 .

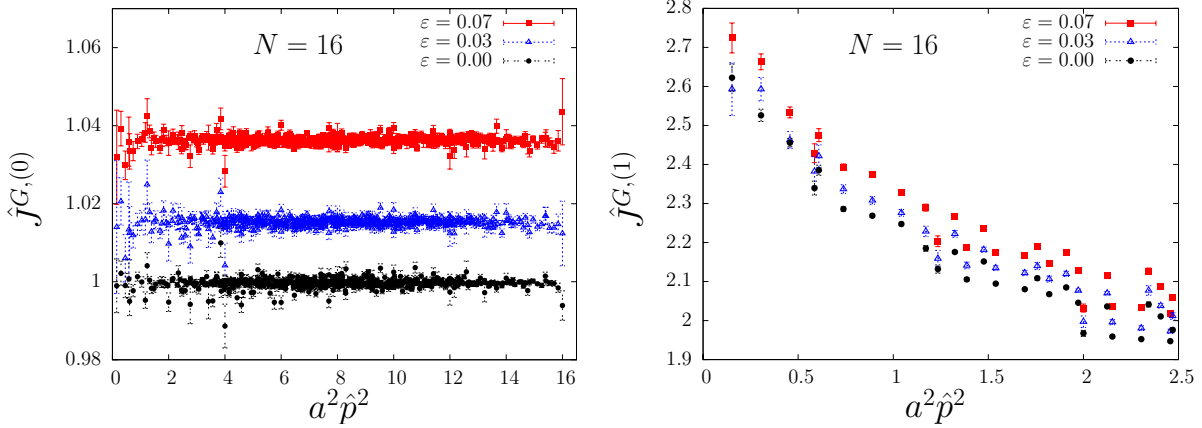


Figure 3: The $\varepsilon \rightarrow 0$ extrapolation of the tree level $\hat{j}^{G,(0)}$ (left) and one-loop $\hat{j}^{G,(1)}$ (right) dressing function vs. $a^2 \hat{p}^2$ at $N = 16$. Note that the one-loop result is shown in a smaller $a^2 \hat{p}^2$ window. The $\varepsilon \rightarrow 0$ extrapolation is reached from above.

5 The perturbative gluon propagator summed to four loops

5.1 Naive summation

Having obtained the different loop contributions to the dressing function in Landau gauge, we can sum up those contributions for a given inverse gauge coupling β to get an estimate of the perturbative gluon propagator.

We calculate the perturbative gluon dressing function at a given lattice volume summed up to loop order n_{\max} for a given lattice coupling β as follows:

$$\hat{j}^G(n_{\max}) = \sum_{n=0}^{n_{\max}} \frac{1}{\beta^n} \hat{j}^{G,(n)} \quad (18)$$

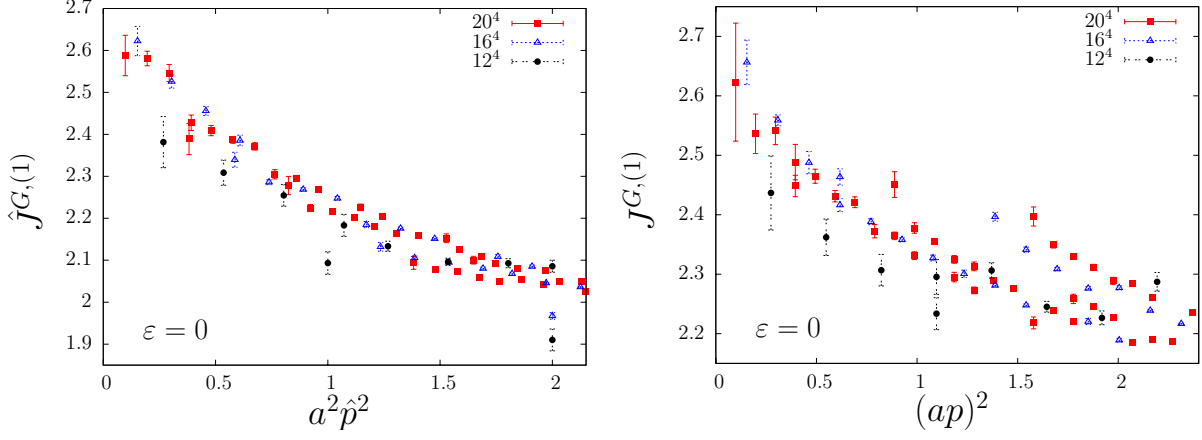


Figure 4: The one-loop dressing functions $\hat{J}^{G,(1)}$ (left) and $J^{G,(1)}$ (right) at selected different volumes vs. small momentum squared $a^2 \hat{p}^2$ and $(ap)^2$.

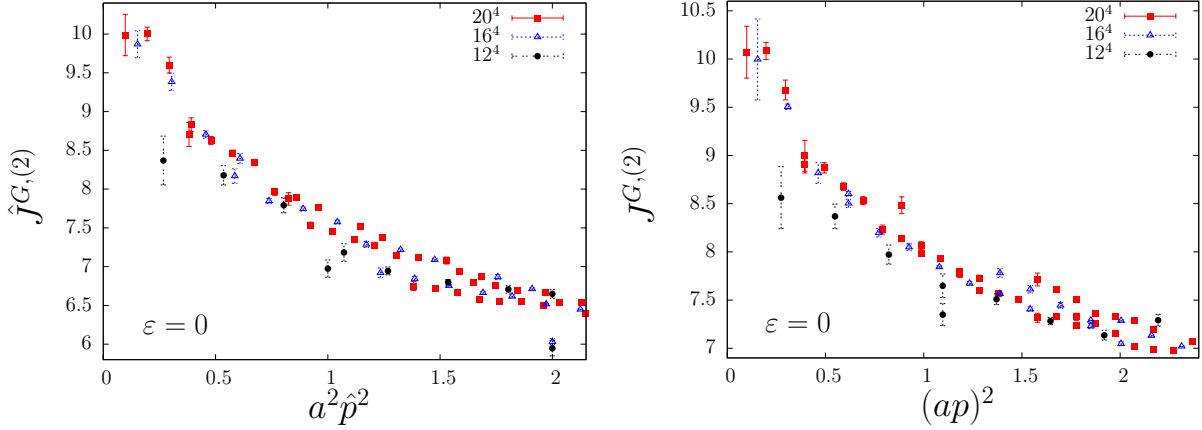


Figure 5: Same as in Fig. 4 for the two-loop dressing functions $\hat{J}^{G,(2)}$ and $J^{G,(2)}$.

and similar for $J^G(n_{\max})$. In contrast to the ghost propagator, here also the tree level “One” is calculated numerically (not shown in the Figures below) and we take the extracted numbers being near to the exact number one.

Restricting ourselves to four-momentum tuples near the diagonal we obtain the following results summarized in Figs. 6 and 7. It is interesting to notice that all loop contributions are of the same sign. Therefore, the summed dressing function most probably represents a lower bound on the complete perturbative dressing function. We have to stress that our perturbative results at large $a^2 \hat{p}^2$ or $(ap)^2$, being at the edges of the Brillouin zones, have nothing to do with the continuum limit in the ultraviolet but could eventually describe the Monte Carlo data in that large lattice momentum region.

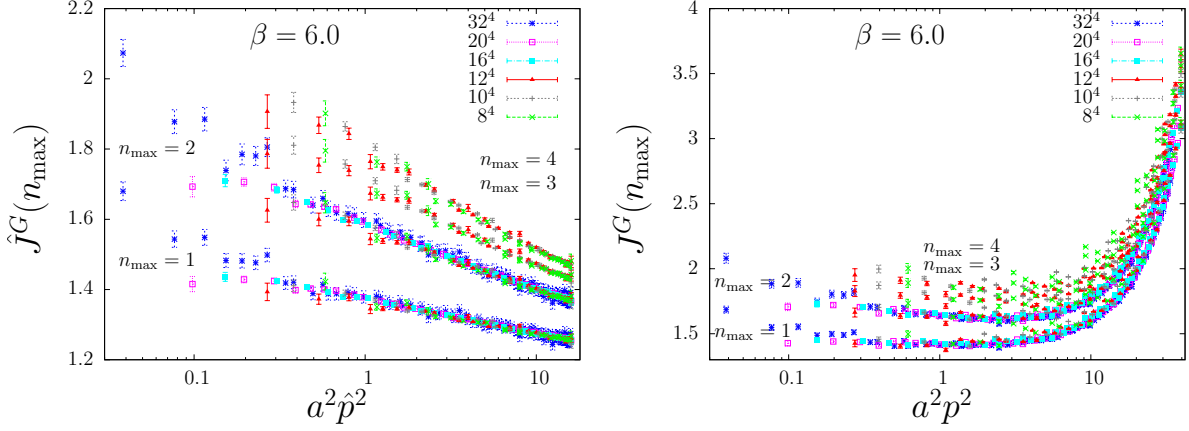


Figure 6: The cumulatively summed perturbative dressing function $\hat{J}^G(n_{\max})$ (left) and $J^G(n_{\max})$ (right) up to four loops (two loops) using $\beta = 6$ at $N = 8, 10, 12$ (16, 20, 32).

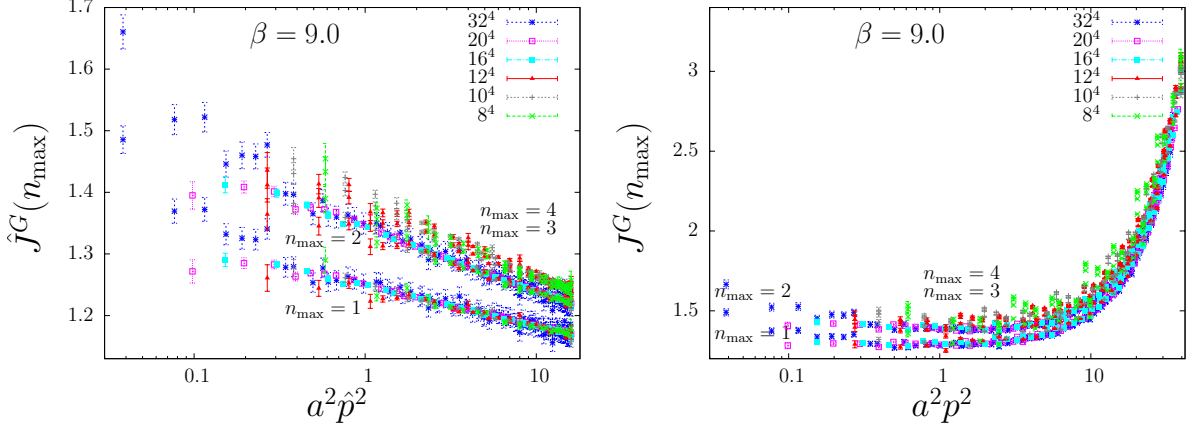


Figure 7: Same as in Fig. 6 at $\beta = 9$.

5.2 Summation using boosted perturbation theory and comparison with Monte Carlo results

It is well-known that the bare lattice coupling $g^2 = 6/\beta$ is a bad expansion parameter. Due to lattice artifacts like non-vanishing tadpole graphs, the lowest order perturbative coefficients are typically very large. Therefore, it has been proposed [34] to use a boosted coupling g_b^2 instead of the bare g^2 to improve the relative convergence behavior. We use here a variant of boosting where g_b^2 is computed via the perturbative plaquette $P_{\text{pert}}(g^2)$ calculated in NSPT (instead of using plaquette measurements from Monte Carlo simulations):

$$g_b^2 = \frac{g^2}{P_{\text{pert}}(g^2)}. \quad (19)$$

Let us expand the perturbative dressing function $\hat{J}^G(n_{\max})$ in g^2 and write

$$\hat{J}^G(n_{\max}) = \sum_{n=0}^{n_{\max}} g^{2n} \hat{j}^{G,(n)}. \quad (20)$$

The analogous expansion in the boosted coupling g_b^2 has the form

$$\hat{J}_b^G(n_{\max}) = \sum_{n=0}^{n_{\max}} g_b^{2n} \hat{j}_b^{G,(n)}. \quad (21)$$

Inserting

$$P_{\text{pert}}(g^2, n_{\max}) = 1 + \sum_{n=1}^{n_{\max}} g^{2n} c_n \quad (22)$$

into (19) we compute the boosted expansion coefficients $\hat{j}_b^{G,(n)}$ as functions of the naive coefficients $\hat{j}^{G,(n)}$ and c_n . For the orders under consideration we thus obtain

$$\begin{aligned} \hat{j}_b^{G,(0)} &= \hat{j}^{G,(0)}, \\ \hat{j}_b^{G,(1)} &= \hat{j}^{G,(1)}, \\ \hat{j}_b^{G,(2)} &= \hat{j}^{G,(2)} + c_1 \hat{j}^{G,(1)}, \\ \hat{j}_b^{G,(3)} &= \hat{j}^{G,(3)} + 2 c_1 \hat{j}^{G,(2)} + (c_1^2 + c_2) \hat{j}^{G,(1)}, \\ \hat{j}_b^{G,(4)} &= \hat{j}^{G,(4)} + 3 c_1 \hat{j}^{G,(3)} + (3 c_1^2 + 2 c_2) \hat{j}^{G,(2)} + (c_1^3 + 3 c_1 c_2 + c_3) \hat{j}^{G,(1)}. \end{aligned} \quad (23)$$

Of course, for the infinite series both expansions should coincide $\hat{J}^G(\infty) = \hat{J}_b^G(\infty)$ – but for every finite, truncated order ($n_{\max} < \infty$) the perturbative series differ. Since the plaquette is less than one, it is clear from (19) that $g_b^2 > g^2$. However, the boosted expansion coefficients become significantly smaller than their naive counterparts, $|\hat{j}_b^{G,(n)}| \ll |\hat{j}^{G,(n)}|$. The combination of both effects results in an improved convergence behavior of the series (21).

An example of such a reordering using (23) is given in Table 3 for $\hat{J}^G(n_{\max} = 4)$ assigned

loop order n	$\hat{j}^{G,(n)}$	$\hat{j}_b^{G,(n)}$
0	0.9804(85)	0.9804(85)
1	0.3638(44)	0.3638(44)
2	0.1995(31)	0.07762(165)
3	0.1296(24)	0.02445(61)
4	0.09070(193)	0.007847(323)

Table 3: Expansion coefficients $j^{G,(n)}$ and $j_b^{G,(n)}$ defined in (20) and (21), respectively, for $\hat{J}^G(n_{\max} = 4)$ assigned to the momentum tuple $(1, 1, 1, 1)$ and the lattice size $N = 12$.

to the momentum tuple $(1, 1, 1, 1)$ at lattice size $N = 12$. For the expansion coefficients of the plaquette in NSPT we use the measured c_n [35]

$$c_1 = -0.334998, \quad c_2 = -0.0337441 \quad c_3 = -0.0137452 \quad c_4 = -0.00729851 \quad (24)$$

for the same lattice size $N = 12$ (neglecting their tiny errors). The two-, three- and four-loop expansion coefficients given in Table 3 are significantly smaller using boosted perturbation theory.

In Figs. 8 we show the effect of boosting for the dressing function $\hat{J}^G(n_{\max} = 4)$ at

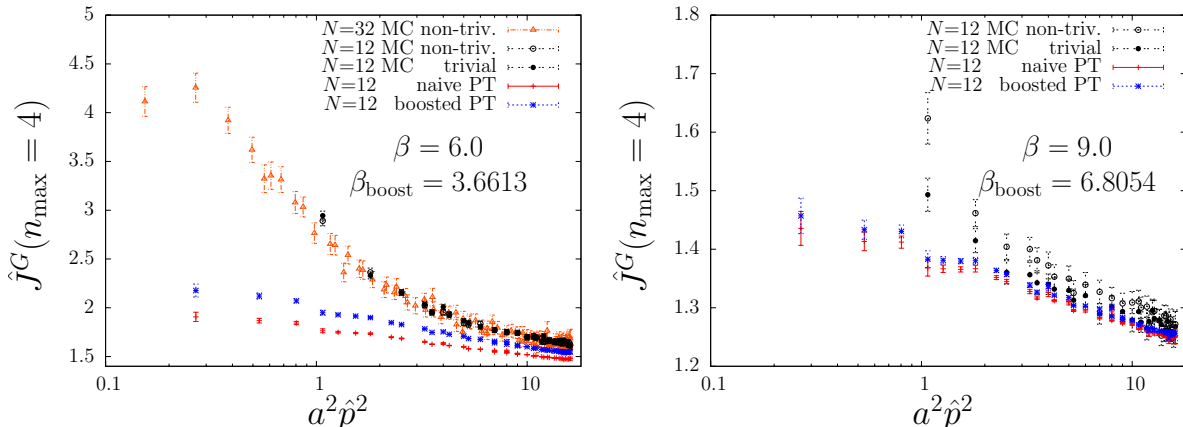


Figure 8: Comparison of naive and boosted perturbation theory for the gluon dressing function at $N = 12$ with Monte Carlo data including real and complex Polyakov loop sectors (non-trivial) and restricted to the real (trivial) Polyakov sector from [36] at two different β values. To show the non-perturbative low momentum behavior, also $N = 32$ Monte Carlo data are included at $\beta = 6$.

two different β values and compare it with Monte Carlo results of the Berlin Humboldt-University group [36] which has used the same gauge field definition (I-6) as implied in NSPT. The boosted result $\hat{J}_b^G(n_{\max} = 4)$ is shifted towards the Monte Carlo results. Note that at the larger β value the Monte Carlo results significantly depend on whether the measurements are restricted to the real (trivial) Polyakov sector. We observe a reasonable agreement of the NSPT summed dressing function at the largest ($a^2\hat{p}^2$) with the Monte Carlo data obtained in the trivial Polyakov sector for all four directions (if necessary, reached by $Z(3)$ flips). For details, see [36].

In contrast to Monte Carlo results [16], we do not see even in higher-loop lattice perturbation theory any sign for a suppression for \hat{J} in the infrared direction (at small $a^2\hat{p}^2$), such that this principal difference must be related to non-perturbative effects responsible for the expected confinement behavior of the gluon propagator. One of interesting questions might be to what extent the difference could be effected by some phenomenological constants. The gluon condensate might be a prominent example.

6 Fit results for LPT in the infinite volume limit

Analogously to paper I we extract the finite constants $J_{i,0}^G$ for loop order i in the perturbative expansion of the lattice gluon dressing function (14) in Landau gauge. We use the same strategy as outlined there.

First we subtract all logarithmic pieces (supposed to be universal and known) from the gluon dressing function for each momentum tuple and for all lattice sizes. Next we select a range in $(ap)^2 = \sum(ap_\mu)^2$, $ap_\mu = k_\mu(2\pi/N)$ with $(ap)_{\min}^2 < (ap)^2 < (ap)_{\max}^2$. Within that range we identify a set of four-momentum tuples (k_1, k_2, k_2, k_4) which is common to all chosen lattice sizes. The data in that set are assumed to have the same $pL = p(aN)$ effects for each given momentum tuple. Since finite-volume effects decrease with increasing momentum squared, we choose as reference fitting point – for an assumed behavior at $N = \infty$ – an additional data point at $(ap)^2 \approx (ap)_{\max}^2$ from the largest lattice size at our disposal. Then we perform a non-linear fit using all data points from different lattice sizes N in that set plus the reference point correcting for finite size (no functional form guessed) and assuming a specific functional behavior for the $H(4)$ dependence. This functional form analogously to (I-62) is a hypercubic-invariant Taylor series (with $(ap)^n = \sum_\mu (ap_\mu)^n$)

$$J_{i,0}^G(ap) = J_{i,0}^G + c_{i,1}(ap)^2 + c_{i,2} \frac{(ap)^4}{(ap)^2} + c_{i,3}(ap)^4 + c_{i,4} \left((ap)^2 \right)^2 + c_{i,5} \frac{(ap)^6}{(ap)^2} + \dots \quad (25)$$

Here $J_{i,0}^G(ap)$ denotes the part of the dressing function which does not depend on $pL = p(aN)$ and logarithmic effects. Finally we vary the momentum squared window and find an optimal χ^2 region which allows us to find the “best” $J_{i,0}^G$.

This time we use our NSPT data – extrapolated to zero Langevin step – from lattice sizes $\{N = 8, 10, 12, 16, 20, 32\}$ for the one- and two-loop case. We take into account tuples with $|k_i - k_j| \leq \Delta k_{\max}$ similar to (I-58). In addition to the ghost propagator case some more tuples are allowed, *e.g.* $\Delta k_{\max} = 2$: $(2,0,0,0)$, $(3,3,1,1)$, \dots

Since we have now a larger lattice volume available when setting the scale as explained in I, the possible optimal fitting window in the momentum squared $(ap)^2$ becomes larger and the number of four-momentum tuples fitted together from all lattices is increased. To get a rough estimate of the three-loop finite constant, we also use the available NSPT measurements from smaller lattice sizes $\{N = 6, 8, 10, 12\}$.

As examples of how the fitting works we present in Figs. 9, 10 and 11 the handling of one-loop, two-loop and three-loop gluon dressing functions at a particular χ^2 value switching off the estimated lattice artifacts in two steps: first the (pL) -effect then the $H(4)$ dependence.

The results for the one-loop constant for ten best χ^2 -values using $\Delta k_{\max} = 2$ are shown in Fig. 12 which agree within errors. The corresponding best two- and three-loop constants for $\Delta k_{\max} = 2$ are given in Fig. 13. Note that for individual χ^2 values the momentum squared windows differ, depending on the number of contributing four-momentum tuples which enter into the non-linear fits.

Table 4 contains a summary of the non-logarithmic constants $J_{i,0}^G$ we have found using three different selection criteria $\Delta k_{\max} = 1, 2, 3$ for the four-momentum tuples. The errors are estimated by equally weighting the mean deviations squared of both the individual fits and the sum of the “best” ten χ^2 values. The results from the different criteria coincide within errors. We have obtained a very good agreement at the level of 0.5 percent with the expected exact one-loop result $J_{1,0}^G$ given in (15).

Comparing the accuracy reached here with that of the ghost propagator, let us mention again that in the gluon propagator case already the tree level is calculated from quantum

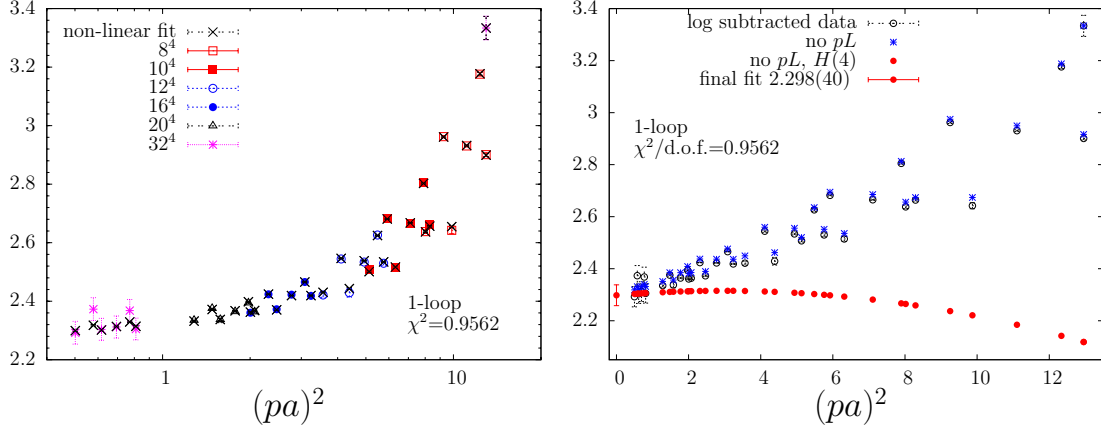


Figure 9: Fitting of the one-loop non-logarithmic coefficient. Left: Data points after subtracting logarithms for various lattice sizes compared to points using the non-linear fit of type (I-66) with (25) analogous to (I-62). Right: Stars denote data after correction for finite-volume effect, the finite volume effect, *i.e.* they represent $J_{i,0}^G(ap)$; full circles are fit points after correcting both finite volume and some hypercubic effects with the exception of those proportional to the coefficients $c_{i,1}$ and $c_{i,4}$ in (25).

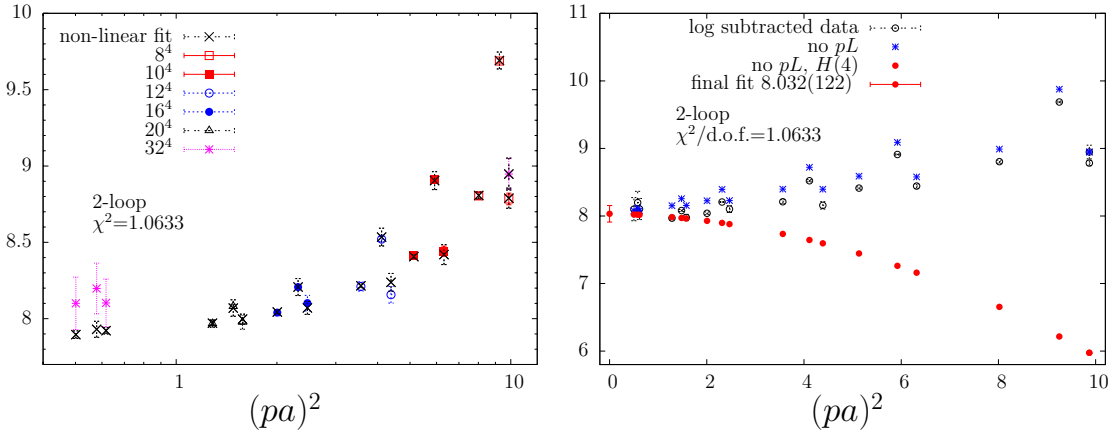


Figure 10: Same as in Fig. 9 for the two-loop non-logarithmic coefficient.

fluctuations of the gauge fields. So the one-loop accuracy in the gluon dressing function case should be fairly compared to the two-loop accuracy of the ghost dressing function.

To estimate the influence of the missing larger volumes for the three-loop constant, let us compare the two-loop constants obtained in the lattice volume sets ($N = 8, \dots, 32$) (one- and two-loop) and ($N = 6, \dots, 12$) (three-loop). The results are collected in Table 5. From the numbers given there we conclude that the missing data sets in the three-loop fit of $\langle J_{3,0}^{G,(3,0)} \rangle$ do not entail a significant change. There is a small tendency to somewhat larger numbers using larger volumes. This has to be taken into account as a systematic effect in our estimate of $J_{3,0}^G$.

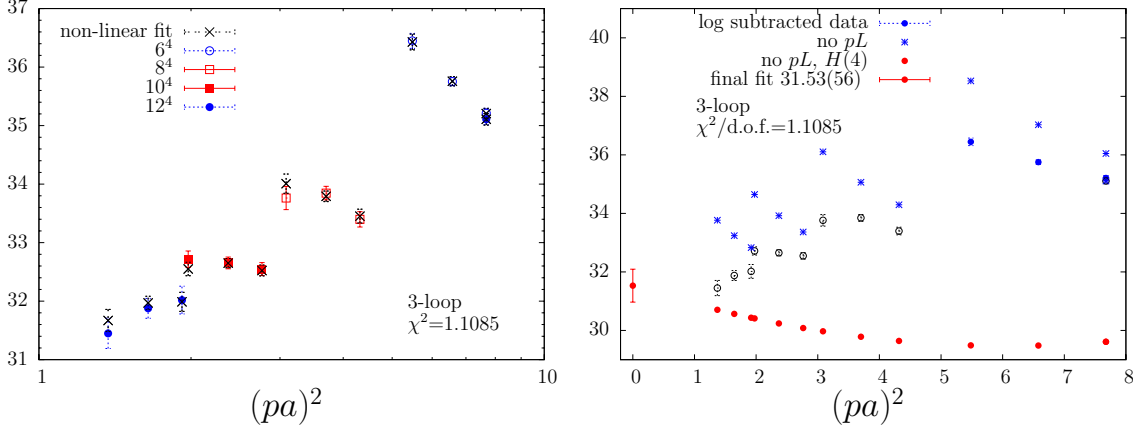


Figure 11: Same as in Fig. 9 for the three-loop non-logarithmic coefficient.

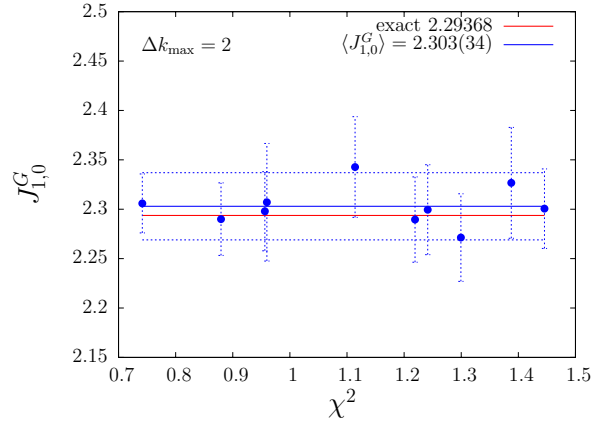


Figure 12: One-loop results $J_{1,0}^G$ allowing $\Delta k_{\max} = 2$ for the smallest available χ^2 together with the exact value 2.29368 (see (15)).

	Δk_{\max}		
	1	2	3
$\langle J_{1,0}^G \rangle$	2.318(56)	2.303(34)	2.292(69)
$\langle J_{2,0}^G \rangle$	7.939(123)	7.927(117)	7.897(112)
$\langle J_{3,0}^G \rangle$	31.61(33)	31.66(47)	31.56(46)

Table 4: Non-logarithmic constants $\langle J_{i,0}^G \rangle$ of the gluon dressing function averaged over the best ten χ^2 values of the non-linear fits using different selection criteria Δk_{\max} for the four-momentum tuples.

Finally we decided to take the selection criterion $\Delta k_{\max} = 2$ as the most suitable one

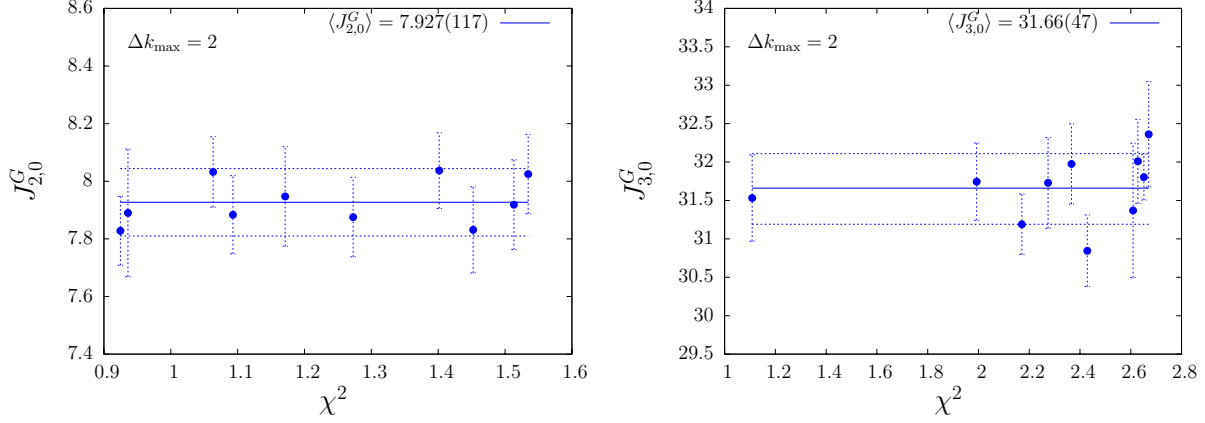


Figure 13: Similar to Fig. 12 for the analytically unknown two-loop and three-loop non-logarithmic coefficients $J_{2,0}^G$ and $J_{3,0}^G$.

Δk_{\max}	$\langle J_{2,0}^G \rangle$ $N = 8, \dots, 32$	$\langle J_{2,0}^G \rangle$ $N = 6, \dots, 12$
1	7.939(123)	7.919(79)
2	7.927(117)	7.876(106)
3	7.897(112)	7.888(115)

Table 5: Comparison of the two-loop constant $\langle J_{2,0}^G \rangle$ using two different lattice volume sets.

and present our numerical results for the unknown non-logarithmic constants in the gluon dressing function of infinite volume lattice perturbation theory in Landau gauge:

$$J_{2,0}^G = 7.93(12), \quad (26)$$

$$J_{3,0}^G = 31.7(5). \quad (27)$$

Collecting all results we can write (14) in a numerical form (restricting to at most five digits after the decimal point)

$$\begin{aligned}
J^{G,3\text{-loop}}(a, p, \beta) = & 1 + \frac{1}{\beta} \left(-0.24697 \log(ap)^2 + 2.29368 \right) + \\
& + \frac{1}{\beta^2} \left(0.08211 \left(\log(ap)^2 \right)^2 - 1.48445 \log(ap)^2 + 7.93(12) \right) + \\
& + \frac{1}{\beta^3} \left(-0.02964 \left(\log(ap)^2 \right)^3 + 0.81689 \left(\log(ap)^2 \right)^2 - 8.13(3) \log(ap)^2 + 31.7(5) \right).
\end{aligned} \quad (28)$$

A transformation to the RI' scheme can be performed using the relations given in Section 3.

7 Summary

In the present work we have applied NSPT to calculate the Landau gauge gluon propagator in lattice perturbation theory up to four loops. The summed gluon dressing function is compared to recent Monte Carlo measurements of the Berlin Humboldt University group. Both (NSPT) perturbative and non-perturbative results are in terms of one and the same definition of the gauge fields, both in Landau gauge fixing and in measurements of the propagator. To improve the comparison, we have also summed our results in a boosted scheme showing better convergence properties.

The key goal of the lattice study of propagators is to reveal their genuinely non-perturbative content, which asks for disentangling perturbative and non-perturbative contributions. The commonly used procedure goes through the fit of the high momentum tail by continuum-like formulae (anomalous dimensions and logarithms can be taken from continuum computation). While this lets us gain intuition, it opens the way to further ambiguities, since irrelevant effects give substantial contributions to the perturbative tail. At large lattice momenta our calculations indicate that the perturbative dressing function constructed by means of NSPT with more than four loops will match the Monte Carlo measurements, thus enabling a fair accounting of the perturbative tail. The strong difference which is left over in the intermediate and – moreover – the infrared momentum region should then be attributed to non-perturbative effects. Power corrections [24] and contributions from non-perturbative excitations [17, 37] are serious candidates for the description of these (better disentangled) effects.

The one-loop result for the perturbative gluon propagator of Lattice $SU(3)$ in covariant gauges (and in particular Landau) has been known for a long time. Using our strategy for a careful analysis of finite volume and finite lattice size effects we find good agreement with this result. In (28) we have summarized our (original) two- and three-loop results.

Acknowledgements

This work is supported by DFG under contract SCHI 422/8-1, DFG SFB/TR 55, by I.N.F.N. under the research project MI11 and by the Research Executive Agency (REA) of the European Union under Grant Agreement number PITN-GA-2009-238353 (ITN STRONGnet).

References

- [1] F. Di Renzo, E.-M. Ilgenfritz, H. Perlt, A. Schiller and C. Torrero, Nucl. Phys. **B 831** (2010) 262 [[arXiv:0912.4152](#) [[hep-lat](#)]].
- [2] R. Alkofer, C. S. Fischer, M. Q. Huber, F. J. Llanes-Estrada and K. Schwenzer, PoS **CONFINEMENT8** (2008) 019 [[arXiv:0812.2896](#) [[hep-ph](#)]].
- [3] L. von Smekal, D. Mehta, A. Sternbeck, and A. G. Williams, PoS **LAT2007** (2007) 382 [[arXiv:0710.2410](#) [[hep-lat](#)]].

- [4] R. Alkofer and L. von Smekal, Phys. Rept. **353** (2001) 281 [arXiv:hep-ph/0007355].
- [5] J. Berges, N. Tetradis, and Ch. Wetterich, Phys. Rept. **363** (2002) 223 [arXiv:hep-ph/0005122].
- [6] J. M. Pawłowski, Annals Phys. **322** (2007) 2831 [arXiv:hep-th/0512261].
- [7] D. Zwanziger, Phys. Rev. **D 69** (2004) 016002 [arXiv:hep-ph/0303028].
- [8] L. von Smekal, R. Alkofer, and A. Hauck, Phys. Rev. Lett. **79** (1997) 3591 [arXiv:hep-ph/9705242].
- [9] L. von Smekal, A. Hauck, and R. Alkofer, Annals Phys. **267** (1998) 1 [arXiv:hep-ph/9707327].
- [10] Ch. Lerche and L. von Smekal, Phys. Rev. **D 65** (2002) 125006 [arXiv:hep-ph/0202194].
- [11] D. Zwanziger, Phys. Rev. **D 65** (2002) 094039 [arXiv:hep-th/0109224].
- [12] D. Zwanziger, Nucl. Phys. **B 412** (1994) 657.
- [13] M. Q. Huber, R. Alkofer, and S. P. Sorella, Phys. Rev. **D 81** (2010) 065003 [arXiv:0910.5604 [hep-th]].
- [14] A. C. Aguilar, D. Binosi, and J. Papavassiliou, Phys. Rev. **D 78** (2008) 025010 [arXiv:0802.1870 [hep-ph]].
- [15] Ch. Fischer, A. Maas, and J. M. Pawłowski, . Annals Phys. **324** (2009) 2408 [arXiv:0810.1987 [hep-ph]].
- [16] A. Sternbeck, E.-M. Ilgenfritz, M. Müller-Preussker and A. Schiller, Phys. Rev. **D 72** (2005) 014507 [arXiv:hep-lat/0506007].
- [17] K. Langfeld, H. Reinhardt, and J. Gattnar, Nucl. Phys. **B 621** (2002) 131 [arXiv:hep-ph/0107141].
- [18] P. O. Bowman, et al., Phys. Rev. **D 78** (2008) 054509 [arXiv:0806.4219 [hep-lat]].
- [19] J. Braun, H. Gies, and J. M. Pawłowski, Phys. Lett. **B 684** (2010) 262 [arXiv:0708.2413 [hep-th]].
- [20] J. Braun, A. Eichhorn, H. Gies, and J. M. Pawłowski, [arXiv:1007.2619 [hep-ph]].
- [21] A. Sternbeck, E.-M. Ilgenfritz, M. Müller-Preussker, A. Schiller, and I. L. Bogolubsky, PoS **LAT2006** (2006) 076 [arXiv:hep-lat/0610053].
- [22] P. O. Bowman, et al., Phys. Rev. **D 76** (2007) 094505 [arXiv:hep-lat/0703022].
- [23] A. Sternbeck, et al., PoS **LAT2007** (2007) 256 [arXiv:0710.2965 [hep-lat]].

- [24] Ph. Boucaud, et al., Phys. Rev. **D 79** (2009) 014508 [[arXiv:0811.2059 \[hep-ph\]](#)].
- [25] A. Sternbeck, et al., PoS **LAT2009** (2009) 210 [[arXiv:1003.1585 \[hep-lat\]](#)].
- [26] B. Blossier, et al., (ETM collaboration), [[arXiv:1005.5290 \[hep-lat\]](#)].
- [27] L. von Smekal, K. Maltman, and A. Sternbeck, Phys. Lett. **B 681** (2009) 336 [[arXiv:0903.1696 \[hep-ph\]](#)].
- [28] E.-M. Ilgenfritz, H. Perlt and A. Schiller, PoS **LAT2007** (2007) 250 [[arXiv:0710.0560 \[hep-lat\]](#)].
- [29] F. Di Renzo, L. Scorzato and C. Torrero, PoS **LAT2007** (2007) 240 [[arXiv:0710.0552 \[hep-lat\]](#)].
- [30] F. Di Renzo, E. Onofri, G. Marchesini and P. Marenzoni, Nucl. Phys. **B 426** (1994) 675 [[arXiv:hep-lat/9405019](#)]; for a review see F. Di Renzo and L. Scorzato, JHEP **0410**, 073 (2004) [[arXiv:hep-lat/0410010](#)].
- [31] H. Kawai, R. Nakayama and K. Seo, Nucl. Phys. **B 189** (1981) 40.
- [32] F. Di Renzo, V. Miccio, L. Scorzato and C. Torrero, Eur. Phys. J. **C 51** (2007) 645 [[arXiv:hep-lat/0611013](#)].
- [33] J. A. Gracey, Nucl. Phys. **B 662** (2003) 247 [[arXiv:hep-ph/0304113](#)].
- [34] G. P. Lepage and P. B. Mackenzie, Phys. Rev. **D 48** (1993) 2250 [[arXiv:hep-lat/9209022](#)].
- [35] E.-M. Ilgenfritz, Y. Nakamura, H. Perlt, P. E. L. Rakow, G. Schierholz and A. Schiller, PoS **LAT2009** (2009) 236 [[arXiv:0910.2795 \[hep-lat\]](#)].
- [36] C. Menz, diploma thesis, Humboldt-Universität zu Berlin (2009); we acknowledge receiving those data prior to publication.
- [37] J. Gattnar, K. Langfeld, and H. Reinhardt, Phys. Rev. Lett. **93** (2004) 061601 [[arXiv:hep-lat/0403011](#)].